Earth Surface Processes and Landforms
Earth Surf. Process. Landforms **25**, 505–518 (2000)

ONE-DIMENSIONAL TRANSITIONAL BEHAVIOUR IN SALTATION

PETER-JOST SPIES[1], IAN K. McEWAN[1]* AND GRAEME R. BUTTERFIELD[2]
[1]*Department of Engineering, University of Aberdeen, Aberdeen, AB24 3UE, UK*
[2]*Department of Geography, Queen Mary and Westfield, Mile End Road, London E1 4NS, UK*

Received 12 January 1998; Revised 23 September 1999; Accepted 21 October 1999

ABSTRACT

One-dimensional simulations of the unsteady saltation process show that the transport rate's response depends on the amplitude and frequency of the wind fluctuations. At frequencies higher than $f \approx 0{\cdot}5$ Hz the transport rate was found not to respond to the wind changes. The initial overshoot reported by previous investigators was found not to appear for simulation heights smaller than 50 to 60 cm. This is due to the fast propagation of the grains' influence upward in the flow and the immediate deceleration of the wind. Confirmation of these findings comes from reports of experiments conducted in wind tunnels of different sizes.

Further test calculations show that the discretization time step size Δt has an influence on the model's temporal behaviour. The reason for this is the better coupling of the wind–sand system when a smaller Δt is used. The implications of bed area choice on the statistical accuracy of predicted transport rate is also demonstrated. In the one-dimensional case the grain cloud's total forward momentum equals transport rate, which is independent of model geometry. Copyright © 2000 John Wiley & Sons, Ltd.

KEY WORDS: wind; sand transport; aeolian sediment transport

INTRODUCTION

After Bagnold (1936) and Kawamura (1951) established their deterministic models of grain trajectories, Owen (1964) was the first to look into the particle–wind interaction with an analytical model. Later, the first computer programs were written relaxing the restricting assumptions of earlier work. Detailed interaction with the wind was investigated in models by Ungar and Haff (1987), Werner (1988, 1990), Anderson and Haff (1991) and McEwan and Willetts (1993) to relate sand transport rate to wind velocity. Whereas the models of Ungar and Haff and Werner used an iterative algorithm to reach the steady state, the models of Anderson and Haff and McEwan used time as the base for the iterations. Thus, they yield a temporal development of the sand–wind system. Sørensen (1991) developed an analytical model to parameterize the transport rate's dependency on wind force. Common assumptions about the air flow close to the ground are a full development of the flow, $\delta/\delta x = 0$, and a simple yet sufficient model for the Reynolds stress, e.g. a mixing length model (Prandtl, 1925). The stratification of the air mass is assumed to be neutral. Any heat effects on the turbulence structure are neglected.

With these assumptions the equilibrium, i.e. the steady state, between the sand grains' forces $f_x(y)$ and the wind is given by:

$$\frac{\partial}{\partial y}\tau(y) = -f_x(y) \tag{1}$$

in which τ is the fluid's shear stress. This equilibrium was described by Owen (1964) as the balance between the fluid's shear stress and the momentum carried by the grain cloud. Integrating Equation 1 between the

* Correspondence to: Dr I. K. McEwan, Department of Engineering, University of Aberdeen, Aberdeen, AB24 3UE, UK. E-mail: i.mcewan@aberdeen.ac.uk
Contract/grant sponsor: Natural Environment Research Council; contract/grant number: GR3/8413

surface and height y yields:

$$\tau(y) - \tau_s = -\int_0^y f_x dy, \tag{2}$$

where the lower limit on the left-hand side is the fluid shear stress at the bed, τ_s. The right-hand side is rewritten;

$$-\int_0^y f_x dy = \int_y^\infty f_x dy - \int_0^\infty f_x dy \tag{3}$$

and we define

$$\tau_g(y) \stackrel{\text{def}}{=} -\int_y^\infty f_x dy \tag{4}$$

as the *grain-borne stress* (Kawamura, 1951). The second term in Equation 3 is the momentum flux from the grain cloud into the sediment bed, $\tau_g(0)$. Using Equation 4 in Equation

$$\tau(y) + \tau_g(y) = \tau_s + \tau_g(0) \tag{5}$$

shows that the profile of the sum of the stresses must be constant throughout the inner region. The value is that of $\tau(\delta_i) = \rho u_{*,\text{eff}}^2$(where $\tau_g(_i) = 0$), termed 'effective shear stress', in order to distinguish it from the bed shear stress. A sketch of the shear stress distribution during steady-state saltation is presented in Figure 1.

THE NUMERICAL MODEL

The numerical model was developed out of the work of McEwan (1991). His model worked from one initial condition towards steady-state Equation 1 in discrete time steps. Instead of solving for the shear stress τ in Equation 1 and further, for the velocities in $\tau = \mu_t \delta\ U/\delta\ y$, where μ_t denotes the turbulent viscosity $\mu_t \delta\ U/\delta\ y = -\rho\overline{\text{uv}}$, the present model uses the discretized *unsteady* boundary layer equation

$$e\frac{\partial U}{\partial t} = \frac{\partial \tau(y)}{\partial y} + f_x(y) \tag{6}$$

and solves for the wind velocity U. The shear stress r is then *explicitly* calculated from the velocity distribution. This approach allows wind velocity fluctuations $\delta\ U/\delta\ t$ to be forced upon the flow.

In their model McEwan and Willetts (1993) used an explicit scheme for temporal changes in the velocity field but only allowed the addition of the (mostly negative) particle sources. A forced velocity change, positive or negative, is not possible. At the upper boundary the fluid shear stress was set in each time step to the sum of grain-borne stress and fluid shear stress at the bed surface (cf. Equation 5). This may be called *Kawamura's boundary condition*. The model of Anderson and Haff (1991) worked in a similar way. Unlike the Aberdeen model, however, their upper boundary condition was a constant shear stress $\tau_\infty = \rho u_*^2$ throughout the whole calculation. The steady state is in both models inevitable because the boundary condition employed describes the equilibrium.

Both models produce a similar temporal behaviour of the grain cloud. A response time of the particles to incipient wind of about 1 s is numerically produced (Anderson and Haff, 1991; McEwan and Willetts, 1993) and also reported from experiments (Butterfield, 1991). A second, longer time scale exists for the adjustment of the wind to the additional roughness of the grain cloud (McEwan and Willetts, 1993). Both scales vary with the imposed u_*. Earlier numerical models (Ungar and Haff, 1987; Werner, 1988, 1990) of the grain cloud did

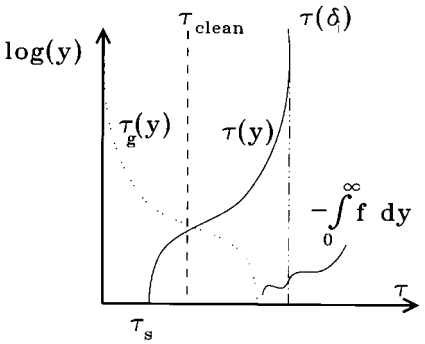

Figure 1. The shear stress profiles during steady-state saltation within the constant stress region. Note that the ordinate is logarithmic. The value for $\tau(\delta_i) = \rho u_{*,\mathrm{eff}}^2$ is the effective shear stress. τ_{clean} is the shear stress distribution in the absence of saltation for the same wind velocity at the boundary layer height. The integral is the flux of forward momentum through the grain cloud $\tau_g(0) = -\int_0^\infty f_x dy$

not use a temporal iteration to reach the steady state. Hence they cannot provide insight into any unsteady behaviour.

Calculation of the wind velocity

The determination of the wind velocities is based on finite volume method described, for example, in Hirsch (1988). In Equation 6 the shear stress is turbulent and a mixing length model is employed to calculate the effective viscosity. Although, strictly speaking, the mixing length model is applicable only to flows with one length scale (Tennekes and Lumley, 1972), it has been successfully used in most models of the saltation layer. Lacking more detailed information Owen (1964) suggested that the mixing length, l, was constant throughout the saltation layer. Tsujimoto *et al.* (1995) evaluated the variations of l using a k–ϵ model. They found an increase in l of up to three times the clean-air value at a height of $y/H \leq 10^{-2}$, where H is the height of the neutral axis ($\tau = 0$) from the bed, which for their calculations was roughly $H \approx 80$ cm. Hence, according to Tsujimoto *et al.*, the mixing length is increased in the lowest 1 cm of the saltation layer. The model presented here, however, neglects the changes in this small portion of the flow and uses a linear relationship $l = ky$ for the mixing length.

Calculation of the grain cloud

The sand cloud is simulated by calculating the trajectories of grains through the flow field. Their momentum exchange with the wind is computed and serves as a source in the calculation of the wind velocities in the next time step. For a one-dimensional model only the vertical distribution, $f_x(y)$, of grain paths is needed. But since the time spent in mid-air depends on the vertical drag as well as the horizontal one, the trajectories should be calculated in both dimensions. Furthermore, a calculation of the particle's x-direction is needed in order to produce a transport rate 'measurement' by counting individual grains passing a certain downwind location.

The aerodynamic particle entrainment was written as an excess shear stress rule (McEwan and Willetts, 1993). If the fluid bed shear stress τ_s exceeds a certain threshold value τ_t, sand grains are introduced into the flow by assigning them a lift-off velocity $\vec{u}_0$ and a uniformly distributed x-location. The grain diameter is chosen randomly from a range of available sizes $d_p \in \{d_{p,1}, d_{p,2}, d_{p,3}\}$.

The number N_e of grains generated per time step and bed area is determined by:

$$N_e = [\Xi A \Delta t(\tau_s - \tau_t)] \tag{7}$$

507in which A is the bed area (bed length L times bed width W) and τ_t is the threshold shear stress for grain motion. The factor Ξ (units: $(\mathrm{N\ s})^{-1} = \mathrm{s\ (m\ kg)}^{-1}$ is an availability, or 'looseness', of sand grains. It can be used to simulate different moisture contents, encrusting or sorting and armouring of the sediment bed. Nickling (1988) gives experimental values for $\Xi\ L$, i.e. counts per unit width and unit time. In these simulations a value of $\Xi = 10^8\ (\mathrm{N\ s})^{-1}$ was applied which reflects the experiments of Nickling.

The product $A\ \Delta t$ determines only the number of aerodynamically entrained grains. Whereas the value of Δt cannot be chosen freely (it influences the accuracy of the coupling between sand cloud and wind, see below), the size of the bed area can be used to determine the number of grains entrained and hence the computational load as well as the statistical accuracy of the computation. To account for situations in which the product $A\ \Delta t$ is too small, yet the shear stress difference large enough for entrainment, a Poisson process is started to launch particles (Kloeden and Platen, 1992). The probability of N_t grains being launched within time t, $P(N_t = k)$, $k = 0, 1, 2, \ldots$ is calculated with:

$$P(N_t = k) = \frac{(\lambda t)^k}{k!} \exp(-\lambda t) \tag{8}$$

in which $\lambda = \Xi\ A\ (\tau_s - \tau_t)$ is the *intensity* of the process. The average number of particles launched within a time t is $\lambda\ t$, which is the value N_e in Equation 7 for $t = \Delta t$.

Grain trajectories are determined by stepwise solving of the equation of motion for a sand grain:

$$\vec{x} = \vec{a} = \vec{g} + \frac{3}{4} C_D(\mathrm{Re}_p) \frac{\rho}{\rho_p} \frac{1}{d_p} \|\vec{U} - \vec{u})\| (\vec{U} - \vec{u}) \tag{9}$$

with $\rho_p = 2650\ \mathrm{kg\ m}^{-3}$ the grain density, C_D the drag coefficient and Re_p the particle Reynolds number.

For the impact process the statistical model described in McEwan *et al.* (1992) was employed rather than calculating the rebound angles from solving the impulse equation for discs, as was done by Rumpel (1985), for example.

Calculation of transport rate

According to its definition, the transport rate, Q, is evaluated in each time step by accumulating the masses m_p of the number, P, of grains passing a specific location and referring to the simulation width W:

$$Q = \frac{1}{W \Delta t} \sum_{i=1}^{P} m_{p,i} \tag{10}$$

This has an important implication for the choice of the computational bed area. Consider two beds each of area $A = 10\ \mathrm{cm}^2$, say, one with the dimensions $L \times W = 10\ \mathrm{m} \times 10^{-4}\ \mathrm{m}$, the other with $L \times W = 1\ \mathrm{cm} \times 10\ \mathrm{cm}$. The number of generated particles per time step is the same for both, but since the latter one is shorter than the average hop length of a sand grain, the transport rate is computed *immediately*, i.e. responds faster than in the other set-up. The longer bed will produce a coarser estimate of Q or even a lag during the first iterations corresponding to number concentration along the bed length and average particle speed. This effect is illustrated in Figure 2 for an effective friction velocity of $u_{*,\mathrm{eff}} = 0{\cdot}3\ \mathrm{m\ s}^{-1}$.

A second method to calculate transport rate was devised in order to avoid the dependency on bed length. By summing up the momentum of all grains. N, in the computational domain and referring to the bed area A, a total momentum snap-shot' (subscript TM) of the grain cloud is produced (McEwan and Willetts, 1994):

$$Q_\mathrm{TM} = \frac{1}{A} \sum_{i=1}^{N} (m_p u_p)_i \tag{11}$$

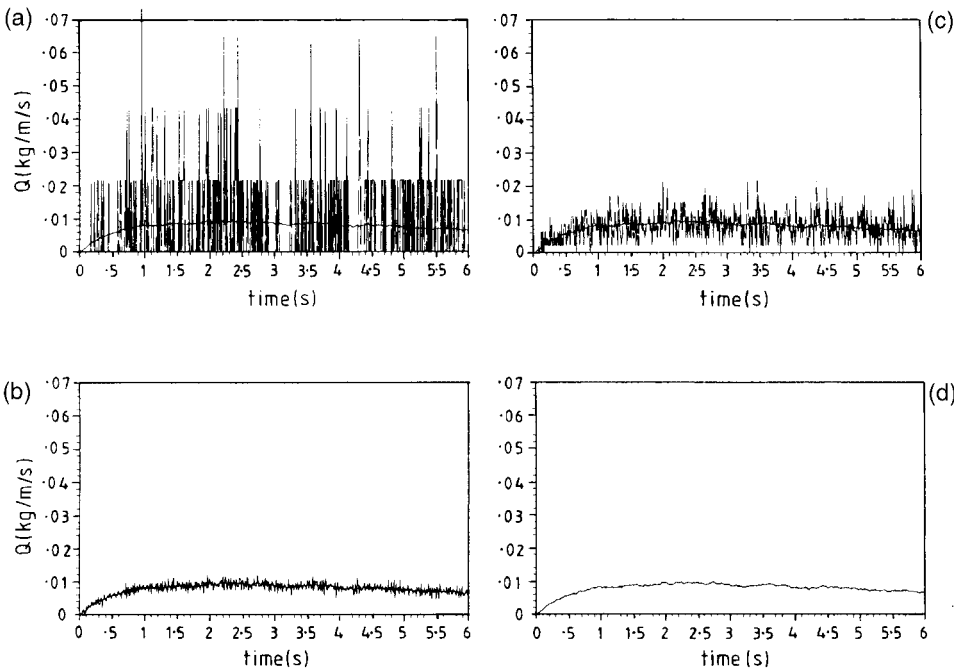

Figure 2. Transport rates computed with different bed lengths (jagged curves) for the same bed area, $A = 10$ cm^2. (a) $L = 10$ m; (b) $L = 1$ m; (c) $L = 10$ cm; (d) $L = 1$ cm. The solid line is the total momentum of the grain cloud, which was the same for all cases. Friction velocity $u_{*,\mathrm{eff}} = 0{\cdot}3$ m s^{-1}

Figure 2 also shows the calculated total momentum (smooth curve, identical for different bed area dimensions) for the tests mentioned. The differences are primarily of stochastic nature, because the sample sizes at the bed end are different. The curve for an extremely short bed ($L = 1$ cm) coincides with the total momentum curve.

It is important to remember that the total momentum is not a mass flux; only for a one-dimensional model does it represent a statistical average of the transport rate. If the momentum in Equation 11 can be approximated with the help of an average grain velocity $\bar{u}_p$, the right-hand side becomes:

$$\frac{1}{LW}\bar{u}_p \sum_{i=1}^{N} m_{p,i} \tag{12}$$

Equating this with the right-hand side of Equation 10 and using $\sum_{i=1}^{K} m_i = K\bar{m}$, we get:

$$\frac{P}{N} \approx \frac{\Delta t \bar{u}_p}{L} \tag{13}$$

as an estimate for the accuracy of the transport rate Q . Since for a given, fixed wind velocity $\bar{u}_p$ is roughly constant, the accuracy is a function of the ratio $\Delta t/L$. Another interpretation of Equation 13 is that of two time scales: the numerical integration step size Δt in relation to a 'particle residence' in the computational domain $L/\bar{u}_p$, i.e. a 'Courant number'.

The preceding analysis is in principle the same as the one presented by McEwan and Willetts (1994, appendix 2) for a uniform grain cloud at steady state. The difference is the application to the numerical model and the estimate 2·8, which refers to the *computational* bed length L unlike the last equation given by McEwan and Willetts which implies a unit length and unit area.

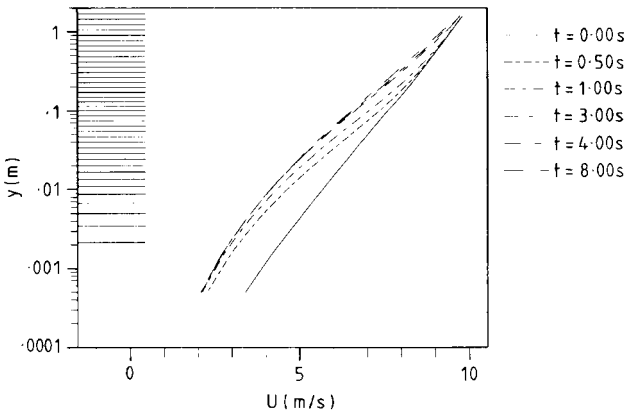

Figure 3. Development of the velocity profiles with time for steady wind with $u_{*,\mathrm{init}} = 0{\cdot}33$ m s^{-1} and $u_{*,\mathrm{eff}} = 0{\cdot}47$ m s^{-1}. The computational grid is marked on the left ordinate.

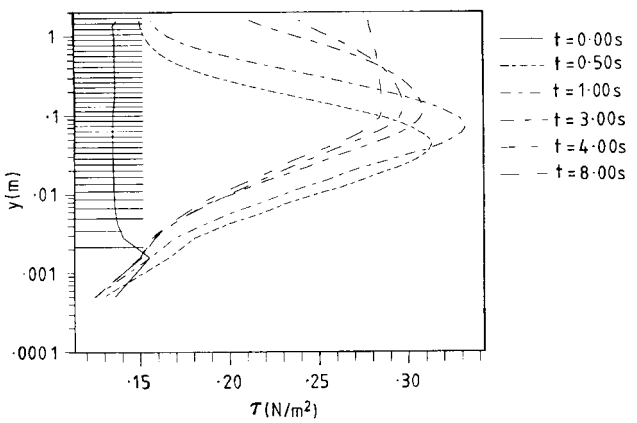

Figure 4. Development of the shear stress profiles with time for steady wind with $u_{*,\mathrm{init}} = 0{\cdot}33$ m s^{-1}; $u_{*,\mathrm{eff}} = 0{\cdot}47$ m s^{-1}

SIMULATION RESULTS

Figures 3 and 4 show the development of wind and shear stress profiles, respectively, predicted for a steady wind of initially $u_{*,\mathrm{init}} = 0{\cdot}33$ m s^{-1} and an effective friction velocity of $u_{*,\mathrm{eff}} = 0{\cdot}47$ m s^{-1}. A simulation height of 2 m was used in these calculations. The wind profile changes show agreement with previously published results for steady-state calculations (McEwan and Willetts, 1991; Anderson and Haff, 1991). The shear stress profiles reveal the slow upward propagation of the maximum. The speed of this variation determines the second time scale before reaching equilibrium.

The sum of shear stress and grain-borne stress is displayed in Figure 5. For larger times ($t > 6$ s) Kawamura's (1951)relation $\tau + \tau_g = \rho u_{*,\mathrm{eff}}^2$ is recovered. It is also seen that this is valid *only* once the equilibrium between grain cloud and wind is obtained, i.e. for the steady state only. Assuming Kawamura's boundary condition for the transitional state is wrong.

The overshooting Q after the initial second is visible in the total stress profile for $t = 1$ s and regression of $r + r_g$ thereafter. However, for smaller simulation heights, equivalent to a smaller wind tunnel height, no overshoot is produced by the model. The graphs is Figure 6 show the transport rate prediction for the first 6 in wind tunnels of different heights. Roughly the same initial friction speed of $u_{*,\mathrm{init}} = 0{\cdot}37$ m s^{-1} was used in all

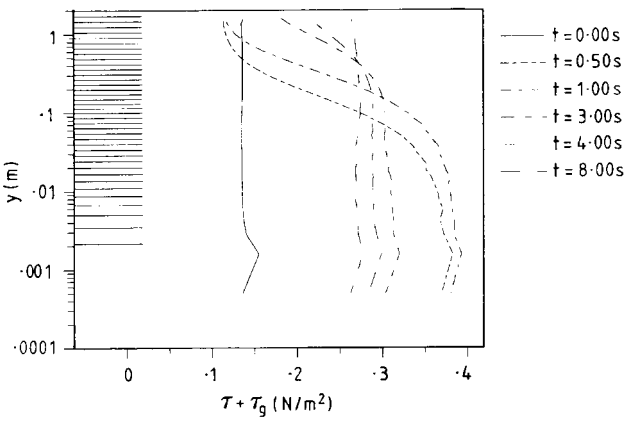

Figure 5. Development of the total stress profiles $\tau + \tau_g$ with time for steady wind with $u_{*,\mathrm{eff}} = 0{\cdot}47\ \mathrm{m\ s^{-1}}$. Kawamura's relation $\tau + \tau_g = \rho u_{*,\mathrm{eff}}^2$ is recovered for large times

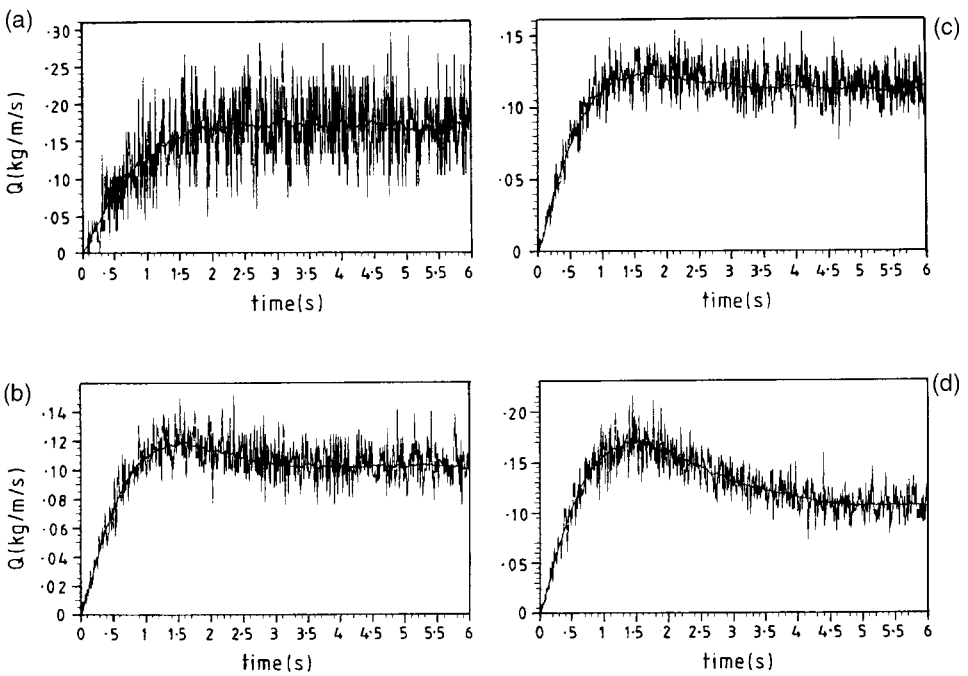

Figure 6. The development of $Q(t)$ for different wind tunnel heights. Tunnel height: (a) 30 cm; (b) 50 cm; (c) 60 cm; (d) 200 cm. The same $u_{*,\mathrm{init}}$ of 37 cm s^{-1} was used in all cases ($u_{*,\mathrm{eff}} \approx 0{\cdot}55\ \mathrm{m\ s^{-1}}$)

cases. The effective friction velocity was around $0{\cdot}55\ \mathrm{m\ s^{-1}}$ once steady state had been obtained. Overshooting of the transport rate is not predicted for tunnel heights of less than 60 cm. The reason for this can be seen by comparing the stress profiles in Figures 7 and 4. The perturbation in the shear stress due to the grains' action reaches the upper boundary faster in a lower tunnel. The whole of the air flow is immediately affected by the momentum exchange. A much quicker feed-back exists between wind and sand.

The numerical experiments previously conducted into the temporal behaviour of the saltation process (Anderson and Haff, 1991; McEwan and Willetts, 1993) use a simulation height of 2 m. Most physical

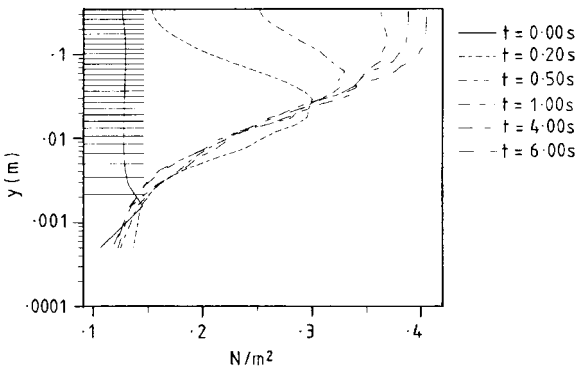

Figure 7. The development of shear stress profiles for a low wind tunnel (height 30 cm). Compare with Figure 4

experiments were conducted in much smaller wind tunnels. Al-Sudairawi (1992) used a tunnel of 50 cm height; he reports no overshoot.

Shao and Raupach (1992) use a duct of height 90 cm and report a very strong peak before equilibrium. However, their data refer to a developing boundary layer and are presented as $Q(t)$ with the help of $t = x/U$, $U \simeq 8{\cdot}7$ m s^{-1}. The results presented in this section (and by earlier steady-state models) show the temporal development of the stationary quantity $Q(x)$ in a *fully developed* flow and should therefore not be compared with Shao's data. The difference between temporal and spatial development is discussed in Spies (1996).

MODEL DEPENDENCY ON TIME STEP SIZE

An important aspect of modelling the saltation cloud with the presented numerical model is the model's dependency on the time step size Δt. The wind velocity is recalculated every Δt seconds. Theoretically, $\Delta t \rightarrow 0$ yields physical behaviour, but this limit is, of course, impracticable. On the other hand, if Δt is chosen too large, the grains' trajectories are computed with a wrong wind profile. In their model, McEwan and Willetts (1993) used a time step size of $\Delta t = 0{\cdot}01$ s, but the particles' flight paths were evaluated with the wind velocity prevailing at lift-off time. So, as for the particle trajectories, the wind update happens after the characteristic flight duration, T. For a friction velocity of $u_{*,\mathrm{eff}} = 0{\cdot}6$ m s^{-1}, $T \approx 0{\cdot}04$ m s^{-1} which is typically $4\Delta t$. Hence there exists a model-implicit inconsistency between trajectory accuracy and wind accuracy. In other words, the system of the two non-linear differential equations

$$\frac{\partial U}{\partial t} = \frac{1}{\rho}\frac{\partial \tau}{\partial y} + a_x(y) \tag{14a}$$

$$a_x(y) = \frac{1}{\rho V}\sum_{i=1}^{N} m_p \ddot{x}(U) \tag{14b}$$

is coupled with two different time scales, T and Δt.

In their model Anderson and Haff (1991) estimate the future number of grain impacts (lift-off time t_1 is known, duration is $T = 2v_0/g$). When the simulation time reaches $t_1 + 2v_0/g$, the trajectory is calculated using a wind profile averaged over $2v_0/g$. The system of Equations 14a and 14b is solved with the two time scales $T = 2v_0/g$ and Δt. Further, trajectories of grains of shorter hop-times are calculated without the influence of long flying grains that exist at the same time.

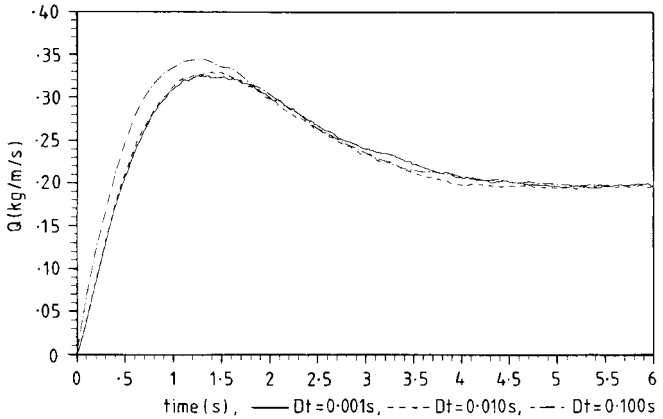

Figure 8. The effect of the time step size on the model's accuracy illustrated for three Δt (0·1 s, 0·01 s and 0·001 s). The graph shows sand transport rate with time. $u_{*,\mathrm{init}} = 0{\cdot}4$ m s^{-1}; $u_{*,\mathrm{eff}} = 0{\cdot}85$ m s^{-1}. For the smallest time step size the overshoot appears earlier than for larger Δt

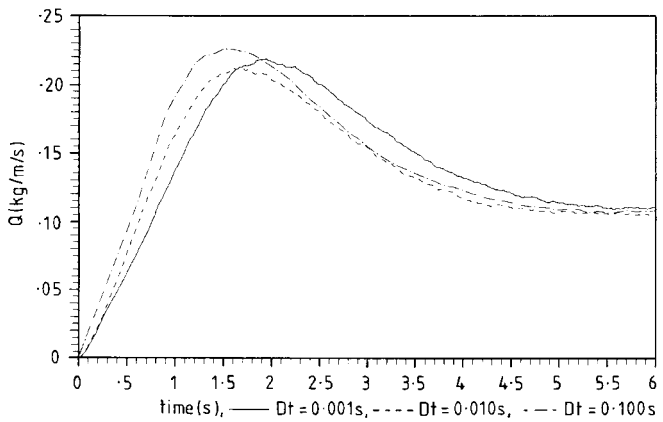

Figure 9. The effect of the time step size on the model's accuracy. In this simulation the rebound angles were explicitly calculated using a disk model (Rumpel, 1985). $u_{*,\mathrm{init}}$ was the same as in the previous graph. For the smallest time step size the overshoot appears 1 s earlier than for larger Δt

In the model presented here, wind and grain cloud are always coupled with the same time scale Δt. To illustrate the effect of variations in Δt on this model's accuracy, the same specifications were used to produce the graphs in Figure 8, the difference being the time step size Δt used. The predicted transport rate at steady state is the same. However, the initial overshoot appears at different times. The difference seems small in this test case. For a different splash function, however, the peak of the overshoot appears up to 1 s earlier if the model is run with the smallest step size (see Figure 9).

Note that the simulation with $\Delta t = 0{\cdot}001$ s is the closest to reality; the computing time of roughly 7 h, however, contrasts with the 50 min needed for the simulation with $\Delta t = 0{\cdot}1$ s.

UNSTEADY-WIND CALCULATIONS

In this section we present results for different wind variations. The energy containing turbulent frequencies of the atmospheric boundary layer appear in the range of 0·01 Hz $\lesssim \omega \lesssim$ 1 Hz (Davenport, 1961; Berman, 1965; Kaimal *et al.*, 1972). In an attempt to simulate the effect of a succession of gusts, a variation in wind

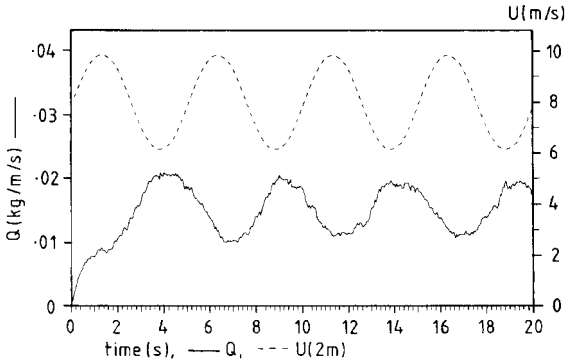

Figure 10. Sinusoidal wind variation imposed on the flow at height 2 m. In this case the mean wind speed was $U_m = 8$ m s^{-1}, which corresponds to a $u_{*,\mathrm{init}} = 0{\cdot}26$ m s^{-1}. The amplitude was $2U_a = 4$ m s^{-1} and period $T = 5$ s

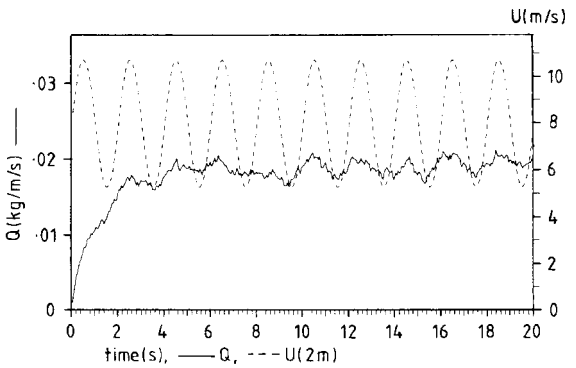

Figure 11. Sinusoidal wind variation imposed on the flow. $U_m = 8$ m s^{-1} ($u_{*,\mathrm{eff}} \approx 0{\cdot}32$ m s^{-1}), $U_a = 3$ m s^{-1}, $T = 2$ s

velocity of different frequency and amplitude was imposed on the upper boundary at height 2 m:

$$U_\infty(t) = U_m + 2U_a \sin(2\pi t/T)$$

in which U_m denotes a mean velocity around which wind fluctuates with amplitude $2U_a$ and period $T = 2\pi/\omega$.

Sinusoidal wind variations

Figure 10 shows a 20 s simulation with a sinusoidal wind variation of $U_m = 8$ m s^{-1}, $U_a = 2$ m s^{-1} and $T = 5$ s ($\omega = 1{\cdot}26$ Hz). After the initial time needed for saturation of the wind, visible in the overshoot at $t = 1{\cdot}2$ s, the transport rate varies with the imposed velocity changes. Due to the initial oversaturation the first peak in Q is greater and broader than subsequent ones. A phase shift of half a cycle is established after the initial period. The response time of Q to the wind changes hence are $1/2T = 2{\cdot}5$ s. The average transport rate was found by integrating $Q(t)$ over the simulation time T_{sim}

$$\bar{Q} = \frac{1}{T_{\mathrm{sim}}} \int_0^{T_{\mathrm{sim}}} Q(t)dt \tag{15}$$

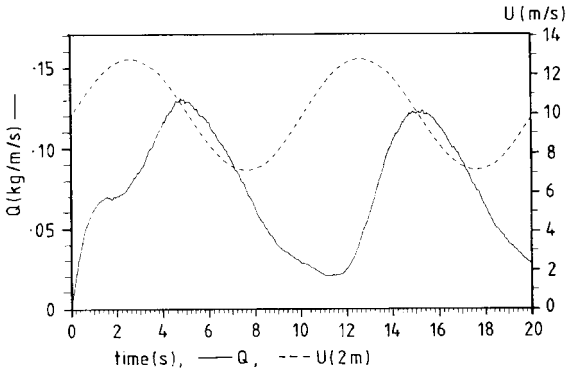

Figure 12. Sinusoidal wind variation imposed on the flow. $U_m = 10$ m s^{-1} ($u_{*,\mathrm{eff}} = 0{\cdot}47$ m s^{-1}), $U_a = 3$ m s^{-1}, $T = 10$ s ($\omega = 0{\cdot}63$ Hz). Two response times, 3 s for the maxima, 4 s for the minima, cause the saw-tooth shape of the graph

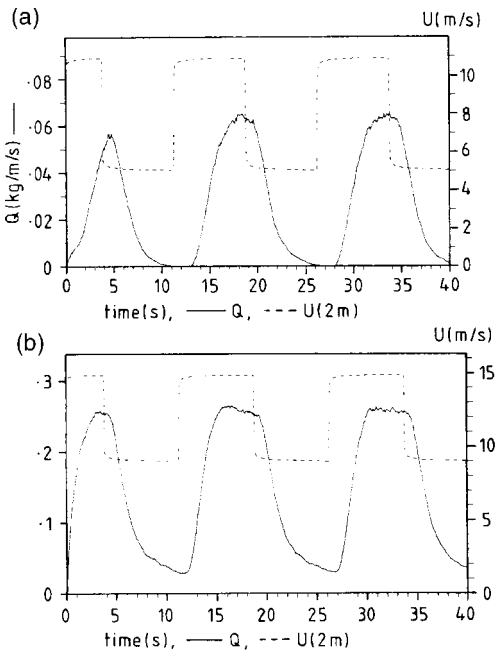

Figure 13. Square wave wind variation imposed on the flows of different base velocity. $U_a = 3$ m s^{-1}, $T = 15$ s. (a) $U_m = 8$ m s^{-1} ($u_{*,\mathrm{eff}} = 0{\cdot}32$ m s^{-1}). (b) $U_m = 12$ m s^{-1} ($u_{*,\mathrm{eff}} = 0{\cdot}60$ m s^{-1}). The magnitude of the base velocity influences the first response to acceleration

to be $\overline{Q} = 0{\cdot}0178$ kg m^{-1} s^{-1}. The average friction velocity is the value for steady wind of $U_m = 8$ m s^{-1}, which is $u_{*,\mathrm{eff}} \approx 0{\cdot}32$ m s^{-1} ($\neq u_{*,\mathrm{init}} = 0{\cdot}26$ m s^{-1}).

At a higher frequency, $\omega = 2\pi/T = 3{\cdot}14$ Hz, which is beyond the typical gust frequencies mentioned above, the variation of Q does not catch up with the wind, see Figure 11. Here a slightly larger amplitude was chosen in order to make smaller variations in Q possible. These do occur with no apparent phase shift. The magnitude of the Q fluctuations is much smaller than in the previous graph and the value of Q remains close to the steady-wind value for $U_m = 9$ m s^{-1} ($u_{*,\mathrm{eff}} \approx 0{\cdot}38$ m s^{-1}) which is $Q = 0{\cdot}02$ kg m^{-1} s^{-1} instead of the value for a steady 8 m s^{-1} wind ($u_{*,\mathrm{eff}} \approx 0{\cdot}32$ m s^{-1}) of $Q = 0{\cdot}007$ kg m^{-1} s^{-1}.

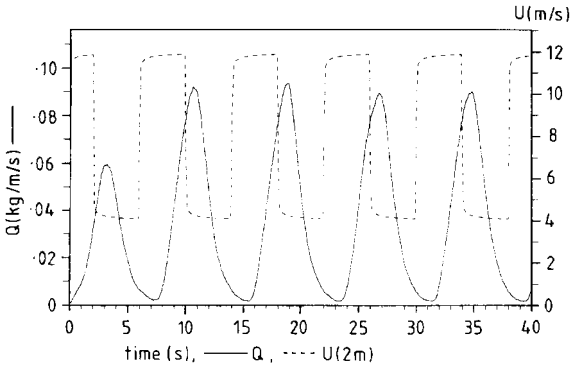

Figure 14. Square wave wind variation imposed on the flow. $U_m = 8$ m s^{-1}, $U_a = 4$ m s^{-1}, $T = 8$ s. The sand cloud responds with a sinusoidal variation because it has no time to reach the equilibrium

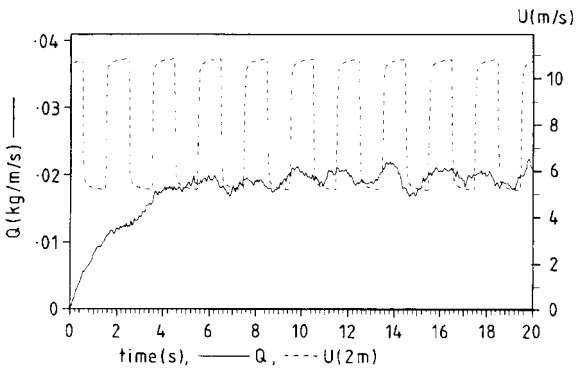

Figure 15. Square wave wind variation imposed on the flow. $U_m = 8$ m s^{-1}, $U_a = 3$ m s^{-1}, $T = 2$ s. The graph of Q is the same as for the sinusoidal variations with the same parameters

The reason for the different response behaviour is the relatively weak coupling of the wind velocity at the upper boundary and the near-surface velocities that drive the sand cloud. This needs to be kept in mind when discussing the effects of gusts on transport rate.

An interesting response of transport rate to the wind changes is shown in Figure 12. The frequency of $\omega = 2\pi/10$ s $= 0{\cdot}63$ Hz is on the high end of the naturally occurring range. The response time is around 3 s for the maximum of Q to a maximum in wind speed. But the response to wind deceleration is about 1 s longer, which causes the saw-tooth shaped curve of $Q(t)$. A longer response time of Q to decelerating wind was also found in wind tunnel experiments (Butterfield, 1991)

Block variation in wind speed

A discontinuously varying wind speed is similar to a succession of steady winds of different velocities. However, the transient behaviour reveals two different response times. In Figure 13 the behaviour of the system to a square wave variation in wind speed is shown. Two base velocities, $U_m = 8$ m s^{-1} and $U_m = 12$ m s^{-1}, were used to create the graphs. The two time scales, the fast response of Q to changes in U and the longer adjustment of U to Q, are seen for every step change made. The magnitude of the base velocity influences the initial response to positive wind change. For the larger U_m a faster response of transport rate is predicted and the first peak in Q reaches its steady-wind value of $Q = 0{\cdot}25$ kg m^{-1} s^{-1}. The sand cloud in a weaker wind

(top graph in Figure 13) does not have enough time to produce the later peak value ($Q = 0{\cdot}06$ kg m^{-1} s^{-1}) in the initial response.

If the frequency is raised beyond a certain limit the sand cloud will never have time to adapt to the wind changes. As a result, the Q variations are sinusoidal in Figure 14. As in the sinusoidal wind variations, no response to wind fluctuations was found for a frequency of $\omega = 3{\cdot}14$ Hz: the graph for $U_m = 8$ m s^{-1}, $U_a = 3$ m s^{-1}, $T = 2$ s (see Figure 15) is almost identical to Figure 11 which had the same specifications.

CONCLUSION

The numerical model presented in this paper is capable of simulating temporal variations in wind speed. The wind velocity is varied with an unsteady upper boundary condition. It reproduces previous investigators' results (Anderson and Haff, 1991; McEwan and Willetts, 1993) for the steady state, the important difference being the complete relaxation of the boundary conditions. No assumption about the stress composition or magnitude at the upper boundary is made. Explicitly evaluated from the velocity distribution, the stress profiles show the slowly upward-propagating maximum. This corresponds to the long time scale found for the wind adjustment to a change in surface roughness.

The model predicts different transient behaviour for different heights of the simulation, i.e. different wind tunnel heights. Wind tunnels lower than 60 cm do not produce the overshoot of transport rate during the onset of the simulation. As was illustrated in Figures 4 and 7, the explanation for this is the considerably stronger coupling between wind and grains for smaller simulation heights. With this finding it can be explained why several experimenters (Bagnold, 1936; Al-Sudairawi, 1992) who used smaller tunnels than this did not report an overshoot.

In the neutral atmospheric surface layer the velocity fluctuations exhibit frequencies of 1 to 10 cycles per minute (Kaimal *et al.*, 1972; Wyngaard, 1992). These gusts have long been suspected of influence on sand transport at least through aerodynamic dislodgement sweeps (Malina, 1941; Anderson *et al.*, 1991; Williams *et al.*, 1994). The characteristic eddy velocity 'felt' near the ground can be as much as 83 per cent of the outer flow velocity U_∞ (Cantwell, 1981).

The unsteady wind simulations (sinusoidal variations as well as square wave changes in velocity) show that transport rate cannot respond fast enough to wind fluctuations with frequencies larger than $f = 0{\cdot}5$ Hz. The model also reveals response times of Q to positive changes in wind velocity of the order of 2 to 3 s. The response to decelerating wind is about 1 s longer. This is in agreement with findings of Butterfield (1991) and Hardisty (1993).

If excited by a fast square wave variation, the cloud undulates in a sine wave manner. If a high-frequency sine wave is driving the wind changes, it Q(t) is almost constant. Since a natural gust is likely to cause an abrupt change in the near-bed wind velocity rather than a smooth one, this result is of importance for the streamwise transportation (advection) of the grain cloud (Spies, 1996).

The legitimacy of relationships $Q \propto u_*$ should be reviewed. Since the friction velocity is an average quantity of the turbulent boundary layer (detailed information about the turbulence structure was lost in obtaining u_*), it cannot itself account for the shape of the fluctuations in wind velocity. Fortunately statistical properties like standard deviation and mean value of the fluctuations scale with $u*$ and further investigation into the influence of wind turbulence on the transport mechanism is suggested.

ACKNOWLEDGEMENTS

The Natural Environment Research Council of the UK provided the financial support for this project under grant number GR3/8413.

REFERENCES

Al-Sudairawi M. 1992. The Effect of Nonerodible Elements on Sand Transport Rate. PhD thesis, University of Aberdeen.

Anderson RS, Haff PK. 1991. Wind modification and bed response during saltation of sand in air. In Acta Mechanica, Vol. Suppl. 1, Barndorff-Nielsen OE, Willetts BB (eds). Springer-Verlag; 21–51, New York.

Anderson RS, Sørensen M, Willetts BB. 1991. A review of recent progress in our understanding of aeolian sediment transport. In Acta Mechanica, Vol. Suppl. 1, Barndorff-Nielsen OE, Willetts BB (eds). Springer-Verlag; New York, 1–19.
Bagnold RA. 1936. The movement of desert sand. *Royal Society, Proceedings* **A157**: 594–620.
Berman S. 1965. Estimating the longitudinal wind spectrum near the ground. *Quarterly Journal of the Royal Meteorological Society* **91**: 302–317.
Butterfield GR. 1991. Grain transport rates in steady and unsteady turbulent air flows. In Acta Mechanica, Vol. Suppl. 1. Barndorff-Nielsen OE, Willetts BB (eds). Springer-Verlag; 97–122, New York.
Cantwell BJ. 1981. Organized motion in turbulent flow. *Annual Review of Fluid Mechanics* **13**: 457–515.
Davenport AG. 1961. The spectrum of horizontal gustiness near the ground in high winds. *Quarterly Journal of the Royal Meteorological Society* **87**: 194–211.
Hardisty J. 1993. Monitoring and modelling sediment transport at turbulent frequencies. In Turbulence: Perspectives on Flow and Sediment Transport, Clifford NJ, French JR, Hardisty J (eds). John Wiley & Sons: Chichester; 35–59.
Hirsch C. 1988. Numerical Computation of Internal and External Flows. Vol. 1, Fundamentals of Numerical Discretization. John Wiley & Sons: Chichester.
Kaimal JC, Wyngaard JC, Izumi Y, Coté OR. 1972. Spectral characteristics of surface-layer turbulence. *Quarterly Journal of the Royal Meteorological Society* **98**: 563–589.
Kawamura R. 1951. Study on Blown Sand by Wind. Technical Report Vol. 5, No. 3/4, Institute of Science and Technology, University of Tokyo (English translation in Research Technical Report HEL-2-8, Hydraulic Engineering Laboratory, University of California, Berkeley, 1964).
Kloeden PE, Platen E. 1992. Numerical Solution of Stochastic Equations. Applications in Mathematics, Vol. 23, Springer, New York.
Malina FJ. 1941. Recent development in the dynamics of wind-erosion. *Transactions of the American Geophysical Union* **22**: 262–286.
McEwan IK. 1991. The Physics of Sand Transport by Wind. PhD thesis, University of Aberdeen.
McEwan LK, Willetts BB. 1991. Numerical model of the saltation cloud. In Acta Mechanica, Vol. Suppl. 1, Barndorff-Nielsen OE. & Willetts BB. (eds). Springer-Verlag, New York.
McEwan IK, Willetts BB, Rice MA. 1992. The grain/bed collision in sand transport by wind. *Sedimentology* **39**: 971–981.
McEwan IK, Willetts BB. 1993. Adaption of the near-surface wind to the development of sand transport. *Journal of Fluid Mechanics* **252**: 99–115.
McEwan IK, Willetts BB. 1994. On the prediction of bed-load sand transport rate in air. *Sedimentology* **41**: 1241–1251.
McEwan IK, Willetts BB, Rice MA. 1992. The grain/bed collision in sand transport by wind. *Sedimentology* **39**: 971–981.
Nickling WG. 1988. The initiation of particle movement by wind. *Sedimentology* **35**: 499–511.
Owen PR. 1964. Saltation of uniform grains in air. *Journal of Fluid Mechanics* **20**: 225–242.
Prandtl L. 1925. Bericht über Untersuchungen zur ausgebildeten Turbulenz. *Zeitschrift für angewandte Mathematik und Mechanik* **5**: 136–139.
Rumpel DA. 1985. Successive aeolian saltation: studies of idealized conditions. *Sedimentology* **32**: 267–280.
Shao Y, Raupach MR. 1992. The overshoot and equilibration of saltation. *Journal of Geophysical Research* **97**(D18):20559–20564.
Sørensen M. 1991. An analytical model of wind-blown sand transport. In Acta Mechanica, Vol. Suppl. 1, Barndorff-Nielsen OE, Willetts BB (eds). Springer-Verlag, New York.
Spies PJ. 1996. The Transport of Sand in Unsteady Winds. PhD thesis, University of Aberdeen.
Tennekes H, Lumley JL. 1972. A First Course in Turbulence. MIT Press: Cambridge (Mass.).
Tsujimoto T, Gotoh H, Nakagawa H. 1995. Momentum exchange between fluid and particles and collisions among particles in saltation layer. In Proceedings of 2nd International Conference on Multiphase Flow, Japan.
Ungar JE, Half PK. 1987. Steady state saltation in air. *Sedimentology* **34**: 289–299.
Werner BT. 1988. A Steady-state Model of Wind-blown Sand Transport. The Blue and White Reports on the Dynamics of Granular Materials **1**. Research Department, Naval Weapons Center, China Lake, California.
Werner BT. 1990. A steady-state model of wind-blown sand transport. *Journal of Geology* **98**: 1–17.
Williams JJ, Butterfield GR, Clark DG. 1994. Aerodynamic entrainment threshold: effects of boundary layer flow conditions. *Sedimentology* **41**: 309–328.
Wyngaard JC. 1992. Atmospheric turbulence. *Annual Review of Fluid Mechanics* **24**: 205–233.

